AIP Journal of Applied Physics

Role of interfacial transition layers in VO2/Al2O3 heterostructures

H. Zhou, M. F. Chisholm, Tsung-Han Yang, S. J. Pennycook, and J. Narayan

Citation: J. Appl. Phys. **110**, 073515 (2011); doi: 10.1063/1.3642980
View online: http://dx.doi.org/10.1063/1.3642980
View Table of Contents: http://jap.aip.org/resource/1/JAPIAU/v110/i7
Published by the American Institute of Physics.

Related Articles

Controlling the fixed charge and passivation properties of Si(100)/Al2O3 interfaces using ultrathin SiO2 interlayers synthesized by atomic layer deposition
J. Appl. Phys. 110, 093715 (2011)

Optical and electrical properties of spray pyrolysis deposited nano-crystalline BiFeO3 films
AIP Advances 1, 042140 (2011)

X-ray nanotomography of SiO2-coated Pt90Ir10 tips with sub-micron conducting apex
Appl. Phys. Lett. 99, 173102 (2011)

Ultrathin ultrananocrystalline diamond film synthesis by direct current plasma-assisted chemical vapor deposition
J. Appl. Phys. 110, 084305 (2011)

S-passivation of the Ge gate stack: Tuning the gate stack properties by changing the atomic layer deposition oxidant precursor
J. Appl. Phys. 110, 084907 (2011)

Additional information on J. Appl. Phys.

Journal Homepage: http://jap.aip.org/
Journal Information: http://jap.aip.org/about/about_the_journal
Top downloads: http://jap.aip.org/features/most_downloaded
Information for Authors: http://jap.aip.org/authors

ADVERTISEMENT

Downloaded 15 Nov 2011 to 128.219.49.14. Redistribution subject to AIP license or copyright; see http://jap.aip.org/about/rights_and_permissions

Role of interfacial transition layers in VO_2/Al_2O_3 heterostructures

H. Zhou,[1,2,a)] M. F. Chisholm,[2] Tsung-Han Yang,[1] S. J. Pennycook,[2] and J. Narayan[1]
[1]*Department of Materials Science and Engineering, North Carolina State University, Raleigh, North Carolina 27695, USA*
[2]*Materials Science and Technology Division, Oak Ridge National Laboratory, Oak Ridge, Tennessee 37831, USA*

(Received 14 June 2011; accepted 18 August 2011; published online 10 October 2011)

Epitaxial VO_2 films grown by pulsed laser deposition (PLD) on *c*-cut sapphire substrates ((0001) Al_2O_3) were studied by aberration-corrected scanning transmission electron microscopy (STEM). A number of film/substrate orientation relationships were found and are discussed in the context of the semiconductor-metal transition (SMT) characteristics. A structurally and electronically modified buffer layer was revealed on the interface and was attributed to the interface free-energy minimization process of accommodating the symmetry mismatch between the substrate and the film. This interfacial transition layer is expected to affect the SMT behavior when the interfacial region is a significant fraction of the VO_2 film thickness. © *2011 American Institute of Physics*. [doi:10.1063/1.3642980]

I. INTRODUCTION

Over the last few decades, vanadium dioxide (VO_2) has attracted extensive research from the basic science community as a correlated electron system and from the applied science community owing to the useful electrical and optical properties resulting from the near room-temperature (~68 °C) semiconductor-metal transition (SMT) the material experiences.[1–3] This property makes VO_2 a favorable candidate for various applications in microelectronics, such as sensing and switching devices.[3] Epitaxial growth of VO_2, therefore, is of significant technological relevance since integration is necessary for applications in microelectronic devices. However, the successful growth of high-quality VO_2 films requires extremely demanding processing conditions. Not only is the substrate selection limited because of the low symmetry of the room temperature VO_2 phase (monoclinic), but also because there are a number of competing oxide phases with different vanadium oxidation states that form as a function of oxygen partial pressure during film growth.[3–5] These oxides have either a much lower transition temperature (e.g., V_2O_3), or a higher transition temperature (e.g., V_3O_5), or even exhibit no SMT transition at all (e.g., V_2O_5).[1,3–5] In addition, the SMT in VO_2 is accompanied by a crystal structure change, from the lower temperature semiconducting monoclinic phase ($P2_1/c$) to the higher temperature metallic tetragonal (rutile) phase ($P4_2/mnm$).[1,2] This crystal structure change further complicates the situation due to the sudden symmetry change of the film across the transition temperature. Nevertheless, epitaxial films of VO_2 have been grown on some single crystal substrates, such as TiO_2 (rutile)[6–9] and α-Al_2O_3.[9–16] The former has the same crystal structure as that of the high temperature VO_2 phase and, thus, would seem to be a suitable substrate candidate. A series of studies has been conducted on this system. It was found that the SMT behavior of VO_2 ultrathin film can be modified by strain introduced by misfit from the substrate.[7,8] Herein, we have used aberration-corrected scanning transmission electron microscopy (STEM), i.e., annular dark field (ADF) imaging and electron energy-loss spectroscopy (EELS), to study the interface region between epitaxial VO_2 films on (0001) Al_2O_3 substrates grown by pulsed laser deposition (PLD). The aberration corrector improved the spatial resolution of the microscope to the sub-angstrom range and therefore permits direct imaging of the interface atomic structure[17–19] as well as revealing the composition and electronic structure of individual columns.[20] We will present in this paper the major results from this study, i.e., the observation of a series of orientation relationships, and a structurally and electronically modified interfacial transition layer. The latter is expected to affect the SMT behavior when the interfacial region is a significant fraction of the VO_2 film thickness.

II. EXPERIMENTAL

VO_2 films were grown on *c*-cut single crystal Al_2O_3 substrates by pulsed laser deposition (PLD) with a KrF excimer laser ($\lambda = 248$ nm) as reported earlier.[14] The deposition temperature was fixed at 600 °C while the oxygen partial pressure was varied from 10^{-1} to 10^{-5} Torr for stoichiometry optimization. X-ray diffraction (XRD) (Rigaku diffractometer, Cu K_α radiation, $\lambda = 1.54$ Å) was used for phase identification as well as a rough estimation of film epitaxial quality. Cross-sectional STEM samples along two in-plane orthogonal zone axes Al_2O_3 $[01\bar{1}0]$ and Al_2O_3 $[2\bar{1}\bar{1}0]$ were prepared by standard mechanical polishing and ion milling. A Nion UltraSTEM (with a 5th order aberration corrector) operated at 100 KeV was used for both ADF imaging and EELS acquisition.

III. RESULTS AND DISCUSSION

A. Structure determination and microstructural characterization

XRD θ-2θ scan results, which are shown in Fig. 1, suggest the optimum oxygen partial pressure for VO_2 epitaxy growth to be in the range of 10^{-1} Torr to 10^{-2} Torr. The

a)Electronic mail: hzhou4@ncsu.edu.

 © 2011 American Institute of Physics

Downloaded 15 Nov 2011 to 128.219.49.14. Redistribution subject to AIP license or copyright; see http://jap.aip.org/about/rights_and_permissions

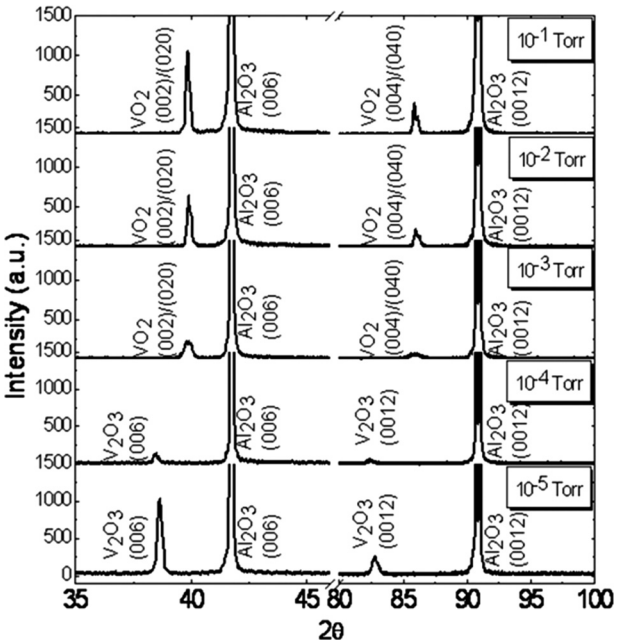

FIG. 1. XRD θ-2θ scan on vanadium oxide films deposited in oxygen partial pressure from 10^{-1} to 10^{-5} Torr. Highly textured VO_2 and V_2O_3 phases are formed depending on the oxygen partial pressures.

films deposited in this range of oxygen pressures only show sharp (002)/(020) and (004)/(040) diffraction peaks, centered at 39.74° and 85.77°, respectively, from the monoclinic VO_2 phase.[2] The (00*l*) and (0*l*0) diffraction peaks of monoclinic VO_2 cannot be distinguished due to their nearly identical d-spacing.[14,15] As the oxygen partial pressure is reduced to 10^{-3} Torr, (002)/(020) has a significantly lowered intensity with a larger full width at half maximum (FWHM), indicating reduced epitaxial quality. When the oxygen partial pressure is reduced to 10^{-4} Torr, the appearance of an epitaxial V_2O_3 phase is suggested by a peak centered at 38.6°, which was identified as the (0006) reflection of V_2O_3. This peak becomes very intense and sharp in the 10^{-5} Torr sample, indicating the formation of a highly textured V_2O_3 phase with V_2O_3 (0001) parallel to Al_2O_3 (0001). The study presented in this paper mainly focuses on the samples deposited at 10^{-1} Torr to 10^{-3} Torr, in which the formation of the monoclinic VO_2 phase was confirmed by XRD. Detailed SMT characteristics for these samples were reported in our earlier papers.[14–16]

Figures 2(a), 2(b), and 2(c) show three representative atomic configurations observed in ADF imaging along the Al_2O_3 [01$\bar{1}$0] zone axis. The less bright columns in the lower part of the images, i.e., the substrate side, are Al and O columns forming the zigzag configuration expected when viewed along the Al_2O_3 [01$\bar{1}$0] direction, as shown in Fig. 2(d) (dashed line is drawn to guide the eyes). The bright columns in the upper part of the images, i.e., the film side, are V columns. The O columns bonded with V atoms are barely visible next to the bright V columns. The three vanadium atomic configurations shown in Figs. 2(a), 2(b), and 2(c) are found to match well with model structures viewed from the VO_2 [100], VO_2 [101] and VO_2 [120] directions (Fig. 2(d)), respectively. Therefore the three corresponding epitaxial

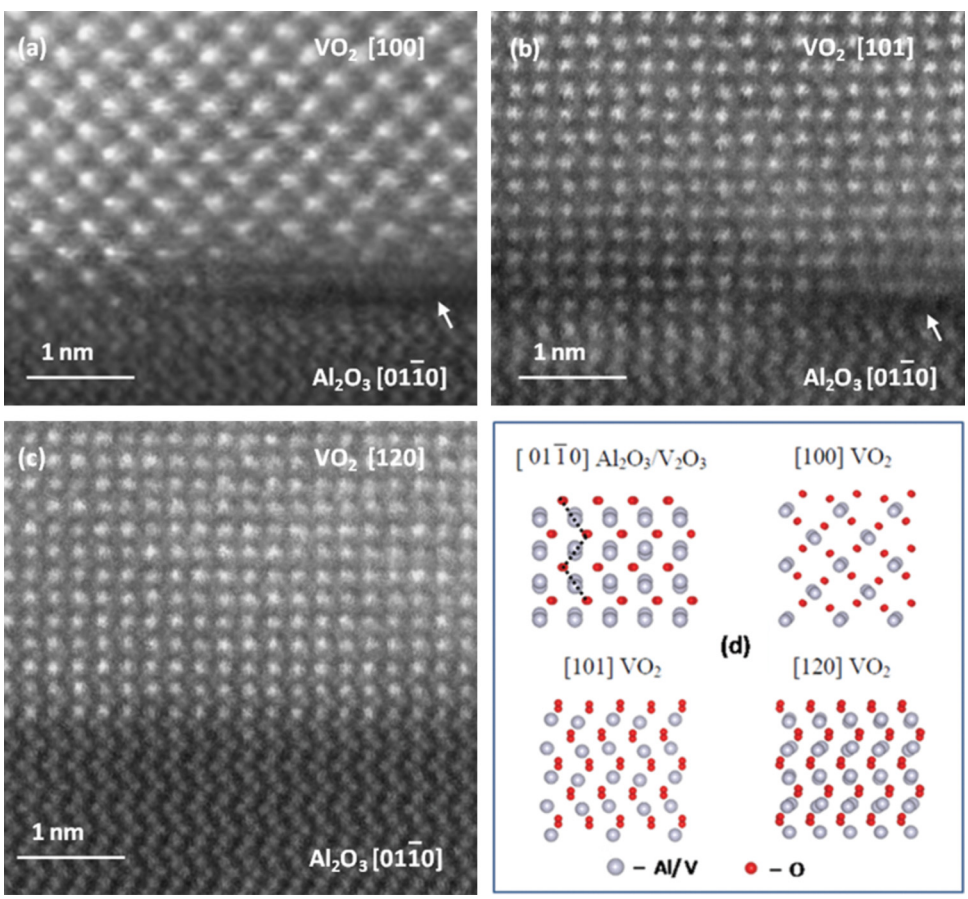

FIG. 2. (Color online) (a), (b), and (c) ADF images of three representative interface atomic configurations along the Al_2O_3 [01$\bar{1}$0] zone axis, which are found to match well with that viewed from VO_2 [100], VO_2 [101] and VO_2 [120] directions (d). The three orientations are therefore determined to be (a) $(010)_M$ or $(001)_M$ of VO_2 // (0001) of Al_2O_3 with in-plane VO_2 $[100]_M$ // Al_2O_3 [01$\bar{1}$0]; (b) $(010)_M$ of VO_2 // Al_2O_3 (0001) with in-plane VO_2 $[101]_M$ // Al_2O_3 [01$\bar{1}$0]; (c) $(001)_M$ of VO_2 // Al_2O_3 (0001) with in-plane VO_2 $[120]_M$ // Al_2O_3 [01$\bar{1}$0]. The oxygen partial pressures under which these samples were deposited are (a) 10^{-1} Torr, (b) 10^{-2} Torr, and (c) 10^{-3} Torr. The arrow in (a) and (b) indicates the "dark" region at the interface. All the images are drift-corrected.

Downloaded 15 Nov 2011 to 128.219.49.14. Redistribution subject to AIP license or copyright; see http://jap.aip.org/about/rights_and_permissions

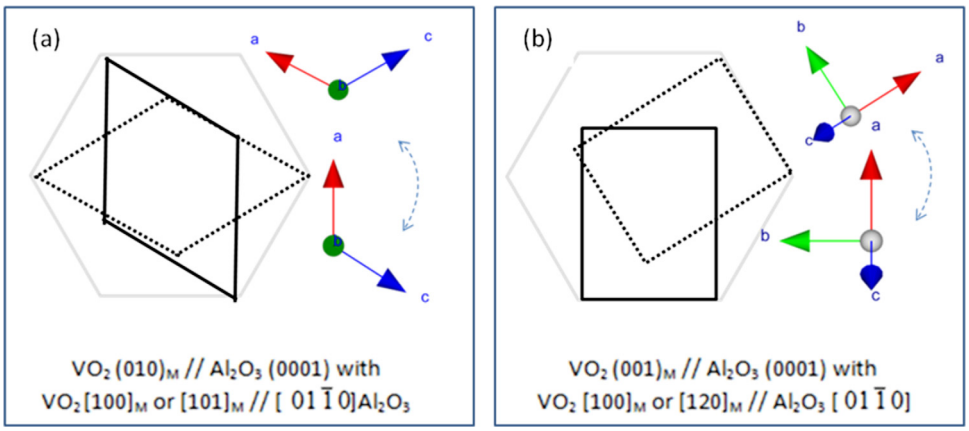

FIG. 3. (Color online) Schematic illustration of the in-plane orientation variants of VO_2 $(010)_M$ // Al_2O_3 (0001) (a) and VO_2 $(001)_M$ // Al_2O_3 (0001) (b). Subscript "M" denotes the monoclinic phase of VO_2.

orientations are determined to be (a) (010) or (001) of VO_2 // Al_2O_3 (0001) with in-plane VO_2 [100] // Al_2O_3 $[01\bar{1}0]$; (b) (010) of VO_2 // Al_2O_3 (0001) with in-plane VO_2 [101] // Al_2O_3 $[01\bar{1}0]$; and (c) (001) of VO_2 // Al_2O_3 (0001) with in-plane VO_2 [120] // Al_2O_3 $[01\bar{1}0]$. Among them, (a) is consistent with those reported earlier,[9–16] while (b) and (c), in a broad sense, can be considered as the in-plane variants (in dashed lines) of the former (solid lines) as shown in Fig. 3. There are three in-plane variants of the same orientation relationship due to the symmetry difference between the rhombohedral corundum Al_2O_3 substrate and monoclinic VO_2 film.[11,12,14,15] Only two of the three are shown in Fig. 3 for clarity.

The coexistence of these orientations originates from the film oxygen sublattice matching that of the substrate during growth and from the subsequent high temperature tetragonal phase transition to the low temperature monoclinic phase that takes place during the cooling process. Figures 4(a) and 4(b) show the atomic configuration of Al_2O_3 (0001) plane and VO_2 $(010)_T$ plane, where subscript "T" denotes the tetragonal phase of VO_2. It is obvious that the oxygen configuration in VO_2 $(010)_T$ can also be regarded as close packed hexagonal, as in (0001) of Al_2O_3, indicated by dashed line hexagon, but with a slightly different degree of distortion. In addition, there are also local similarities in the relative

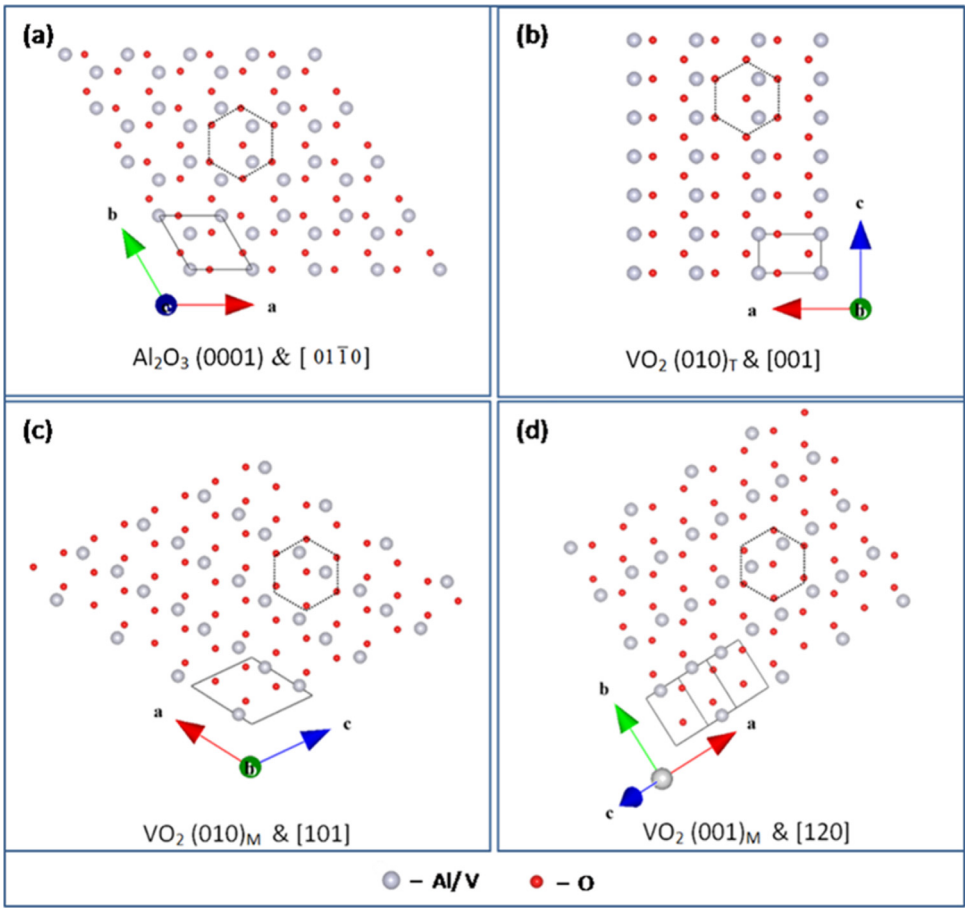

FIG. 4. (Color online) Atomic configurations of relevant planes: Al_2O_3 (0001) (a), VO_2 $(010)_T$ (b), VO_2 $(010)_M$ (c), and VO_2 $(001)_M$ (d), where subscripts "M" and "T" denote the monoclinic phase and tetragonal phase, respectively. VO_2 $(010)_M$ in (c) and VO_2 $(001)_M$ in (d) are positioned with respect to Al_2O_3 (0001) depicting the corresponding in-plane alignment in orientations shown in Figs. 1(b) and 1(c), respectively. It should be noted that in all VO_2 planes, oxygen atoms are slightly corrugated along the plane normal.

Downloaded 15 Nov 2011 to 128.219.49.14. Redistribution subject to AIP license or copyright; see http://jap.aip.org/about/rights_and_permissions

TABLE I. The six epitaxial orientations deduced from oxygen sublattice matching between tetragonal VO_2, monoclinic VO_2 and *c*-cut Al_2O_3 (the indices listed indicate the corresponding parallel lattice planes and in-plane directions).

Al_2O_3	(0001) & [01$\bar{1}$0]					
Parallel plane & direction in tetragonal VO_2	(100) & [001]	(100) & [011]	(100) & [01-1]	(010) & [001]	(010) & [101]	(010) & [10-1]
Parallel plane & direction in monoclinic VO_2	(001) & [100]	(001) & [1-20]	(001) & [120]	(010) & [100]	(010) & [001]	(010) & [101]

position of the cations, i.e., Al and V, with respect to that of the anion (O). The $(100)_T$ of VO_2 is identical to $(010)_T$ and therefore is not shown. From the point view of interfacial free-energy minimization, it is expected that film orientations that provide maximum preservation of the oxygen sublattice continuity across the interface should develop, provided sufficient ad-atom mobility is present. This means the epitaxial growth can only proceed by stacking these planes, i.e., $(100)_T$ or $(010)_T$ of VO_2. Either way, the film *c*-axis lies in the growth plane. The tendency to preserve the oxygen sublattice continuity across the interface also determines the in-plane orientation since these hexagon edges should be aligned as much as possible. It is this oxygen sublattice alignment that leads to the three in-plane variants. Since *a* and *b* are interchangeable in tetragonal structure, the three in-plane variants derived when $(100)_T$ VO_2 // (0001) Al_2O_3 are equivalent to those derived from $(010)_T$ VO_2 // (0001) Al_2O_3. In Fig. 4, VO_2 $(010)_T$ is positioned with respect to Al_2O_3 (0001) depicting one of the latter orientation relationships. The tetragonal to monoclinic phase transition that takes place during the cooling process differentiates these two sets of orientation variants. The low temperature monoclinic phase forms by pairing vanadium ions along *c*-axis followed by an *ab* plane shearing of the high temperature phase.[2,21] The *a*-axis of monoclinic phase originates from the *c*-axis of tetragonal phase with its lattice constant doubled: $a_M = 2c_T$, where subscript "M" and "T" denotes the monoclinic phase and the tetragonal phase, respectively. With the *c*-axis of tetragonal phase always lying in the epitaxial growth plane, the *ab* plane shearing in the tetragonal phase determines whether the new *c*-axis (monoclinic phase) is in the growth plane or out of the growth plane. This leads to two sets of possible orientations for the monoclinic phase, i.e., $(010)_M$ VO_2 // (0001) Al_2O_3 and $(001)_M$ VO_2 // (0001) Al_2O_3, with each having three in-plane variants as listed in Table I. The orientations from both sets were observed in our study as shown in Figs. 2(b) and 2(c), which are schematically illustrated in Figs. 3(a) and 3(b) (in dashed lines) as well in Figs. 4(c) and 4(d), where VO_2 $(010)_M$ and VO_2 $(001)_M$ are positioned with respect to Al_2O_3 (0001) depicting the corresponding in-plane alignment. On the one hand, this suggests that energetically there is no strongly preferred shearing direction during the phase transition. On the other hand, it also demonstrates the heterogeneous nature of the phase transition in thin film VO_2.[22,23] Indeed, in which way the transition proceeds could be significantly affected by microstructural defects and local strain conditions, which might considerably modify the nucleation barriers.

ADF imaging along another zone axis, Al_2O_3 [2$\bar{1}\bar{1}$0], provides additional important data on the interfacial reaction between VO_2 and Al_2O_3. This specific [2$\bar{1}\bar{1}$0] zone axes is perpendicular to the [01$\bar{1}$0] zone axis described earlier. As shown in Figs. 5(a) and 5(c), while in the substrate side (lower part of the image), Al columns pair up forming dumbbell shapes aligned at an angle to the interface, as expected when viewed from any Al_2O_3 [2$\bar{1}\bar{1}$0] zone axis, one noticeable feature on the film side is the loss of column alignment a few monolayers away from the interface. This confirms the orientations determined earlier. Along this zone axis, except for the orientation shown in Fig. 2(a), where $(010)_M$ or $(001)_M$ of VO_2 // Al_2O_3 (0001) with in-plane VO_2 $[100]_M$ // Al_2O_3 [01$\bar{1}$0], this viewing direction in the other orientations are all high index directions with no clearly resolved atomic columns. The most distinguishable feature in many of the ADF images taken along this direction is an interface region, where the lattice is seen to be the same as that of Al_2O_3 (*R-3c*) with the heavier V atoms in the Al atom positions. The lattice in these regions is identified as that of V_2O_3 since above 150 K, V_2O_3 has a rhombohedral corundum crystal structure, the same as that of Al_2O_3. This interface region is not obvious in the images taken from the orthogonal zone axis, Al_2O_3 [01$\bar{1}$0], because of the close match of the V configuration in VO_2 viewed from the [101] and [120] directions to that in V_2O_3 viewed from the [01$\bar{1}$0] direction, as shown in Fig. 2(d). It should be noted that the zigzag pattern is not visible in V_2O_3 due to the significantly enhanced intensity of cation columns, i.e., vanadium, relative to Al. This layer was more or less observed in all VO_2 films, regardless of the oxygen partial pressure under which the film was deposited. Therefore, it is reasonable to conclude that its formation is related to the templating effect from the substrate since this region continues/preserves the crystal structure of the Al_2O_3 substrate. The overwhelming influence of the substrate symmetry on the initial stage of vanadium growth has been reported earlier in surface studies.[6,24] It was found that in the sub-monolayer coverage regime, vanadium has a strong tendency to preserve the substrate surface long-range structure order by occupying selective surface sites, e.g., sixfold-coordinated titanium sites, which underbridge oxygen atoms of the topmost layer when grown on rutile TiO_2 (110) surface,[6] and aluminum vacancies when grown on a stable Al_2O_3 (0001) surface.[24] Thus during the initial growth stage chemical free-energy dominates before strain free-energy associated with planar mismatch takes over during rest of the epitaxial growth process.[13]

B. EELS and bonding characteristics studies

The atomic resolution EELS investigation on the interface region reveals a certain degree of non-stoichiometry. Vanadium is one of the metals in the first transition period, and its unfilled 3d bands are strongly hybridized with O 2p

Downloaded 15 Nov 2011 to 128.219.49.14. Redistribution subject to AIP license or copyright; see http://jap.aip.org/about/rights_and_permissions

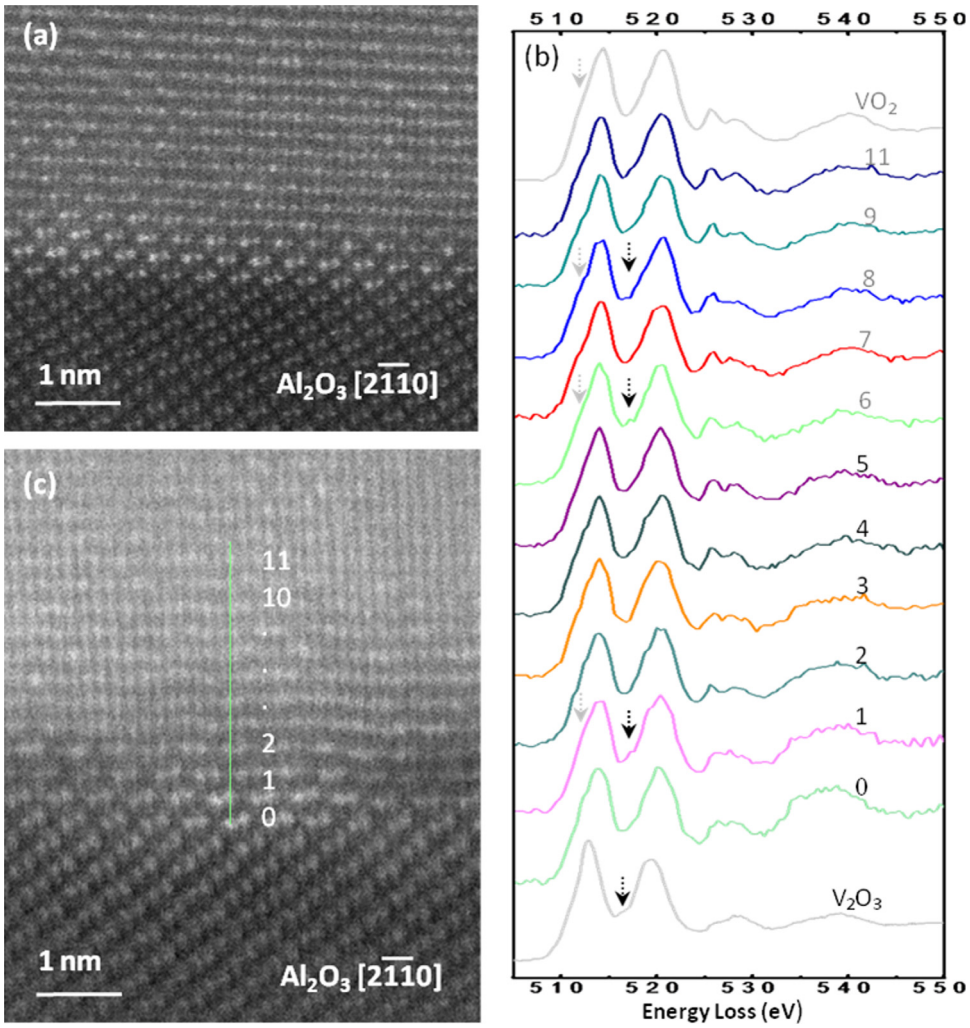

FIG. 5. (Color online) (a) An ADF image of the interface along the Al_2O_3 [2$\bar{1}\bar{1}$0] zone axis. (b) A series of electron energy loss (EELS) spectra acquired along the direction perpendicular to the interface, labeled in order from "0" to "11" with "0" acquired at the "V_2O_3" –like interface region and "11" acquired inside the film (acquisition time 1 s and energy dispersion 0.4 eV per channel). The vertical line in (c) roughly marks the region where the series of spectra was acquired. EELS from VO_2 (top) and V_2O_3 (bottom) are also included in (b) for comparison. Gray and dark arrows in (b) indicate the V^{4+} and V^{3+} signature, respectively.

bands in vanadium oxides. Therefore, as in other transitional metal oxides, both the V-$L_{2,3}$ edges (also called white lines) and the O-K edge are expected to reflect the V oxidation state. Figure 5(b) shows a series of spectra acquired along the direction perpendicular to the interface, labeled in order from "0" to "11" with "0" acquired at the "V_2O_3"–like interface region and "11" acquired about three nanometers into the film, as roughly marked by a vertical line in Fig. 5(c). The acquisition time is 1 s for each position and the energy dispersion used is 0.4 eV per channel, leading to an energy resolution around 1 eV. EELS from VO_2 (top) and V_2O_3 (bottom) are included for comparison. These two spectra were taken from films grown with the highest and lowest oxygen partial pressures. They are found to be very similar to those reported from standard (stoichiometric) compounds.[25,26] In general, L_3 and L_2 edges are expected to shift to higher energy as oxidation state increases, e.g., a 1.2 eV shift is reported going from V_2O_3 to VO_2.[26] Therefore, in Fig. 5(b), the spectrum from VO_2 (top) and V_2O_3 (bottom) are aligned with the series of spectra using the first peak in O-K edge. The background was removed in front of V-$L_{2,3}$ edge using the power-law method in Gatan's Digital Micrograph. The first two strong peaks around 514 eV and 520 eV are V-L_3 and V-L_2, which in a first approximation, are attributed to excitation from V $2p_{3/2}$ and V $2p_{1/2}$ to unoccupied V 3d states, respectively.[26] The remaining peaks belong to the O-K edge. The doublets around 525–529 eV are attributed to excitations from O 1s to hybridized O 2P – V 3d bands with $t_{2\ g}$ and e_g symmetry, respectively.[25] The much broader peak centered around 539 eV is attributed to excitations from O 1s to the hybridized O 2p - V 4sp.[25]

This series of spectra suggests a certain degree of nonstoichiometry near the interface. On the one hand, it is apparent that on moving from the VO_2 film to the interface, the V $L_{2,3}$ edges, in terms of L_3/L_2 intensity ratio and position, are essentially unchanged implying that the V oxidation state is unchanged, i.e., maintaining 4+, despite the fact that the crystal takes the V_2O_3 structure at the interface. On the other hand, the change in the near-edge fine structure of O-K is obvious on moving from the VO_2 film to the interface. The decreasing trend of the relative weight of t_{2g} over e_g is similar to that from VO_2 (top) to V_2O_3 (bottom), which is consistent with a V_2O_3 structure at the interface. The latter is not surprising since the O-K edge, especially, the first peak(s) near the threshold (the so-called prepeak), is very sensitive to local chemical bonding environment.[25] The first peak (t_{2g}) in O-K edge corresponds to excitation to O 2p hybridized with V 3d orbitals that point in between the ligands forming

Downloaded 15 Nov 2011 to 128.219.49.14. Redistribution subject to AIP license or copyright; see http://jap.aip.org/about/rights_and_permissions

weak π anti-bonds and the second peak (e_g) corresponds to the excitation to O 2p hybridized with V 3d orbitals that points toward the ligands forming strong σ anti-bonds.[27] In this interfacial "V_2O_3" region, vanadium and its nearest neighbor oxygen forms VO_6 octahedra that are supposedly more highly anion sharing than in the VO_2 lattice, and therefore stronger σ anti-bonding is expected, which leads to a reduced relative weight of t_{2g} over e_g.

Furthermore, some spectra near the interface show signatures for both V^{4+} and V^{3+}, i.e., the bump at the shoulder of the low energy loss side of the V-L_3 peak, and the small bump at the foot of the low energy loss side of the V-L_2 peak,[26,28] as indicated by gray and dark arrows in Fig. 5(b), respectively. This indicates the possibility of co-existence of V^{4+} and V^{3+} in the lattice in a region extending beyond the "V_2O_3" interfacial layer. It is speculated that some mixed valence oxide has formed near the interface region following the interfacial non-stoichometric V_2O_3 phase. The main driving force comes from the competition between interface strain energy and chemical free energy. For epitaxial growth, the mismatch between the film and substrate comes from differences in lattice spacing and lattice vector. The latter originates from the symmetry difference across the interface and is relatively harder to accommodate than the former, which is easily accommodated by misfit dislocations.[29] The initial growth of the "V_2O_3" lattice at the interface, although highly defective, eliminates the symmetry mismatch at the interface. Once away from the substrate, e.g., a few monolayers, the film structure and composition should be driven to that of stoichiometric equilibrium phase, VO_2. Hence, there is still the same amount of symmetry mismatch that needs to be accommodated. The detection of a co-existence of V^{4+} and V^{3+} in the region extending beyond the "V_2O_3" interfacial layer suggests that this symmetry mismatch might be accomplished through local octahedral distortion in a transition region. In vanadium oxide crystal, the building unit can be considered as VO_6 octahedra in which vanadium is covalently bonded with its six nearest-neighbor oxygens. Oxygen octahedra in the V_2O_3 (V^{3+}) structure are less distorted than those in VO_2 (V^{4+}) since the former are more highly anion sharing. It can be envisaged that during the initial stage of growth, minimization of strain energy requires less distorted octahedra stacked in the same way as V_2O_3, while minimization of chemical energy favors distorted octahedra that are connected like those in VO_2. There are a series of mixed valence oxides, V_nO_{2n-1}, the so-called Magnéli phases, between V_2O_3 and VO_2 in the temperature range studied.[5] The crystal structure of these mixed valence phases can be considered to be formed by crystallographic shearing from the structures of these single valence phases with the driving force coming from the correlation of point defects, e.g., oxygen vacancies in VO_2 or vanadium vacancies in V_2O_3, provided they are densely populated as a result of non-stoichometry. The crystal structures of these phases show structural affinity to both VO_2 and V_2O_3 as they contain rutile-like and corundum-like blocks.[5] For example, V_3O_5, as the closest neighbor of V_2O_3 in this family, has crystal structures containing double octahedral (formed by two single octahedra sharing a face),[30] which is also the building unit of V_2O_3. It is speculated that some mixed valence oxides are formed, at least locally, to fulfill this symmetry transition from corundum to rutile. A similar evolution of octahedral distortions in the interface region imposed by symmetry mismatch has been reported in epitaxial perovskite oxide interface.[31,32]

Finally, many regions of the interface appear dark in the 10^{-1} Torr and 10^{-2} Torr samples, as shown in Figs. 2(a) and 2(b) indicated by arrows. Although the exact nature of this dark region is not well understood, its origin is speculated to be a poorly bonded interface and to be related to the tetragonal to monoclinic phase transition. The symmetry reduction during the transition requires a change in the V-O bond length and direction at the interface. Therefore, a highly strained/disordered region can be expected considering the limited atom mobility at the transition temperature ($\sim$68 °C). Interestingly, in the 10^{-3} Torr sample the film is seen to remain well bonded with the substrate, as shown in Fig. 2(c), despite the reduced epitaxial quality revealed by XRD. This is probably because an oxygen deficient deposition environment benefits a wider transition region due to a reduced driving force that pushes the film to stoichiometric VO_2 (Ref. 11) and therefore the strain/disorder induced by the VO_2 phase transition could be spread out over a larger region near the interface. While possibly improving the heterostructure interface, the existence of this transition region might modify the SMT behavior if the thickness of VO_2 is reduced significantly, for example, to a value comparable to the thickness of the transition region, where the defects and therefore the strain accumulated, and fragments of mixed valence oxides, if any, could considerably alter SMT behavior.

IV. CONCLUSION

In summary, the epitaxial VO_2/*c*-Al_2O_3 heterostructure was studied by aberration-corrected STEM. Atomic ADF imaging revealed a series of orientations, which can be traced back to oxygen sublattice matching and the tetragonal to monoclinic phase transformation. A V_2O_3-like phase, with a thickness of a few monolayers, is also found at some interface regions. Atomic resolution EELS study reveals a structurally and electronically modified transition region, which is attributed to the interface self-optimization process involving chemical and strain free energies of accommodating the symmetry mismatch between the substrate and the film.

ACKNOWLEDGMENTS

This research was supported by the National Science Foundation (Grant No. DMR-0803663) (H.Z., T.-H.Y., J.N.) and DOE Office of Science, Materials Sciences and Engineering Division (M.F.C., S.J.P.). Schematic drawings presented in this paper were produced using *Vesta*.[33]

[1]F. J. Morin, Phys. Rev. Lett. **3**, 34 (1959).
[2]J. B. Goodenough, J. Solid State Chem. **3**, 490 (1971).
[3]J. Nag and R. F. Haglund, Jr., J. Phys.: Condens. Matter **20**, 264016 (2008), and references therein.
[4]C. H. Griffiths and H. K. Eastwood, J. Appl. Phys. **45**, 2201 (1974).
[5]U. Schwingenschlögl and V. Eyert, Ann. Phys. **13**, 475 (2004).
[6]M. Sambi, G. Sangiovanni, G. Granozzi, and F. Parmigiani, Phys. Rev. B **54**, 13464 (1996).

Downloaded 15 Nov 2011 to 128.219.49.14. Redistribution subject to AIP license or copyright; see http://jap.aip.org/about/rights_and_permissions

[7]K. Nagashima, T. Yanagida, H. Tanaka, and T. Kawai, J. Appl. Phys. **101**, 026103 (2007).
[8]Y. Muraoka, Y Ueda, and Z. Hiroi, J. Phys. Chem. Solids **63**, 965 (2002).
[9]H. L. M. Chang, H. You, J. Guo, and D. J. Lam, Appl. Surf. Sci. **48/49**, 12 (1991).
[10]G. Garry, O. Durand, and A. Lordereau, Thin Solid Films **453**, 427 (2004).
[11]I. Yamaguchi, T. Manabe, and T. Tsuchiya, Jpn. J Appl. Phys. **47**, 1022 (2008).
[12]Z. P. Wu, S. Yamamotoy, A. Miyashitay, Z. J. Zhang, K. Narumiz, and H. Naramotoz, J. Phys.: Condens. Matter **10**, L765 (1998).
[13]J. Narayan and V. M. Bhosle, J. Appl. Phys. **100**, 103524 (2006).
[14]T.-H. Yang, C. Jin, R. Aggarwal, R. J. Narayan, and J. Narayan, J. Mater. Res. **25**, 422 (2010).
[15]T.-H. Yang, R. Aggarwal, A. Gupta, H. Zhou, R. J. Narayan, and J. Narayan, J. Appl. Phys. **107**, 053514 (2010).
[16]T.-H. Yang, S. Nori, H. Zhou, and J. Narayan, Appl. Phys. Lett. **95**, 102506 (2009).
[17]S. J. Pennycook and L. A. Boatner, Nature **336**, 565 (1988).
[18]S. J. Pennycook and D. E. Jesson, Phys. Rev. Lett. **64**, 938 (1990).
[19]S. J. Pennycook and D. E. Jesson, Ultramic. **37**, 14 (1991).
[20]N. D. Browning, M. F. Chisholm, and S. J. Pennycook, Nature **366**, 143 (1993).
[21]P. Baum, D.-S. Yang, and A. H. Zewail, Science **318**, 788 (2007).
[22]R. Lopez, T. E. Haynes, L. A. Boatner. L. C. Feldman, and R. F. Haglund, Jr., Phys. Rev. B **65**, 224113 (2002).
[23]J. Y. Suh, R. Lopez, L. C. Feldman, and R. F. Haglund, Jr., J. Appl. Phys. **96**, 1209 (2004).
[24]J. Biener, M. Baümer, R. J. Madix, P. Liu, E. Nelson, T. Kendelewisz, and G. Brown, Jr., Surf. Sci. **449**, 50 (2000).
[25]C. Hébert, M. Willinger, D. S. Su, P. Pongratz, P. Schattschneider, and R. Schlögl, Eur. Phys. J. B **28**, 407 (2002), and references therein.
[26]A. Gloter, V. Serin, C. Turquat, C. Cesari, C. Leroux, and G. Nihoul, Eur. Phys. J. B **22**, 179 (2001), and references therein.
[27]M, Abbate, H. Pen, M. T. Czyiyk, F. M. F. de Groat, J.-C. Fuggleav, Y. J. Ma, C. T. Chen, F. Sette, A. Fujimori, Y. Ueda, and K. Kosuge, J. Elec. Spec. Rel. Phen. **62**, 185 (1993).
[28]M. G. Brik, K. Ogasawara, H. Ikeno, and I. Tanaka, Eur. Phys. J. B **51**, 345 (2006).
[29]J. Narayan and B. C. Larson, J. Appl. Phys. **93**, 278 (2003).
[30]S.-H. Hong and S. Åsbrink. Acta. Cryst. B **38**, 713 (1982).
[31]A. Y. Borisevich, H. J. Chang, M. Huijben, M. P. Oxley, S. Okamoto, M. K. Niranjan, J. D. Burton, E. Y. Tsymbal, Y. H. Chu, P. Yu, R. Ramesh, S. V. Kalinin, and S. J. Pennycook, Phys. Rev. Lett. **105**, 087204 (2010).
[32]J. He, A. Y. Borisevich, S. V. Kalinin, S. J. Pennycook, and S. T. Pantelides, Phys. Rev. Lett. **105**, 227203 (2010).
[33]K. Momma and F. J. Izumi, Appl. Crystallogr. **41**, 653 (2008).

Downloaded 15 Nov 2011 to 128.219.49.14. Redistribution subject to AIP license or copyright; see http://jap.aip.org/about/rights_and_permissions